Journal of Alloys and Compounds 685 (2016) 418–422

Contents lists available at ScienceDirect

Journal of Alloys and Compounds

journal homepage: http://www.elsevier.com/locate/jalcom

# Structure and dielectric properties of $Nd(Zn_{1/2}Ti_{1/2})O_3 - BaTiO_3$ ceramics for energy storage applications

Wen-Bo Li [a], Di Zhou [a, b, *], Bin He [a], Fei Li [a], Li-Xia Pang [c], Sheng-Guo Lu [d]

[a] Electronic Materials Research Laboratory, Key Laboratory of the Ministry of Education & International Center for Dielectric Research, Xi'an Jiaotong University, Xi'an 710049, Shaanxi, China
[b] Xi'an Jiaotong University Suzhou Academy, Suzhou 215123, Jiangsu, China
[c] Micro-optoelectronic Systems Laboratories, Xi'an Technological University, Xi'an 710032, Shaanxi, China
[d] School of Materials and Energy, Guangdong University of Technology, Guangzhou 510006, China

ARTICLE INFO

*Article history:*
Received 22 March 2016
Received in revised form
17 May 2016
Accepted 28 May 2016
Available online 30 May 2016

*Keywords:*
Sintering
Ceramic
$Nd(Zn_{1/2}Ti_{1/2})O_3$
$BaTiO_3$
Energy storage property

ABSTRACT

In this work, a full range of compositions of $(1-x)Nd(Zn_{1/2}Ti_{1/2})O_3-xBaTiO_3$ (NZT-BT) ($0.0 \leq \times \leq 1.0$) ceramics were prepared by using conventional solid state reaction method at sintering temperature from 1300 °C to 1500 °C. Sintering behavior, phase composition, microstructures, and energy storage properties were investigated. X-ray diffraction (XRD) analysis showed that the system formed a monoclinic solid solution when $0 < x < 0.3$, a cubic perovskite solid solution when $0.5 < x < 0.9$, a tetragonal perovskite solid solution when $0.94 < x < 1.0$. Materials were found to be ferroelectric when $x \geq 0.9$. The $0.08\ Nd(Zn_{1/2}Ti_{1/2})O_3-0.92BaTiO_3$ ceramic sample was found to possess the largest energy density about 0.62 $J/cm^3$ with charging efficiency 90% at a breakdown field strength 131 kV/cm.



## 1. Introduction

With the increasing demands for compact electronics in modern electronics and electrical power systems such as hybrid electric vehicles (HEV), medical defibrillators, filters, and switched-mode power supplies, high energy storage density dielectric materials have become a major enabling technology [1–7]. Dielectric materials with high energy density would help to reduce the volume, weight, and cost of power system [7–12]. It is well known that the energy storage density ($J$) is determined by the dielectric constant and the breakdown strength (BDS):

$$J = \int EdD \tag{1}$$

where J is the total stored energy density, E is the applied electric field and D is the electric displacement. For linear dielectrics, $J = 1/2DE = 1/2\varepsilon_r\varepsilon_0E^2$, where $\varepsilon_r$ is the dielectric constant of the ceramic materials and $\varepsilon_0$ is the vacuum permittivity [12–17]. Therefore, J strongly depends on the $\varepsilon_r$ and E, where E is limited by the breakdown strength ($E_b$). In order to reach a high energy density, characteristics such as high dielectric constant, high breakdown strength and low dielectric loss are needed for dielectric materials [18–22]. Conventionally, anti-ferroelectric ceramic dielectrics synthesized by solid-state reaction method are selected as medium voltage capacitors owing to their extremely high dielectric constant. However, their applications are limited by several property degradations, such as the low breakdown strength (BDS) caused by interior defect of pores during the sintering route and their high remnant polarization leading to a very small polarization difference in the polarization–electric field (P–E) loop [21–24]. This is a serious problem about the energy conversion efficiency in anti-ferroelectric ceramics. Recently, many efforts have been focused on improving the energy storage properties of $BaTiO_3$ (BT), $SrTiO_3$ (ST) and $Pb(Zr,Ti)O_3$ (PZT) based ceramic so as to attain high energy storage density capacitors, such as using compositions with Curie temperatures (determined from temperature corresponding to the maximum dielectric constant) well below the operating temperature, optimization of the microstructure, addition or doping in the glass ceramics and so on [25–28].

$BaTiO_3$ (BT) ceramic plays a key role in the field of energy

* Corresponding author. Electronic Materials Research Laboratory, Key Laboratory of the Ministry of Education & International Center for Dielectric Research, Xi'an Jiaotong University, Xi'an 710049, Shaanxi, China.
*E-mail address:* zhoudi1220@gmail.com (D. Zhou).

http://dx.doi.org/10.1016/j.jallcom.2016.05.311
0925-8388/

density capacitors because of its high permittivity, high breakdown strength and favorable bias stability. The noble metal Sc has been used to improve the temperature stability of the $BaTO_3$ ceramics in energy-storage application, i.e., $0.7BaTiO_3$–$0.3BiScO_3$ ceramics, which exhibit energy density of 6.1 J/cm$^3$ at field of 73 kV/mm [28]. The substitution of A-site or B-site ion can reduce the remnant polarization of BT-based ceramics effectively. The properties of $Ba_{0.4}Sr_{0.6}TiO_3$ (0.37 J/cm$^3$ under 120 kV/cm) and $BaTiO_3$–$Ba(Mg_{1/3}Nb_{2/3})O_3$ (BT–BMN) composite ceramic (1.07 J/cm$^3$ under 158 kV/cm) have been reported [29–32]. Pure $Nd(Zn_{1/2}Ti_{1/2})O_3$ (NZT) sintered at 1500 °C exhibiting excellent microwave dielectric properties (a permittivity of ~27.5, a quality factor Qf of ~27,000 GHz and a temperature coefficient of frequency of (TCF or $\tau_f$) ~ −53 ppm/ C) is one of the good candidates to form a solid solution with BT ceramic due to the similar crystal structure [32]. The ionic radius of $Ba^{2+}$ (1.43 Å) is a little larger than that of $Nd^{3+}$ (1.27 Å) and NZT can diffuse into the BT lattices to form a solid solution. Due to the different thickness and breakdown strength, the energy storage densities of ceramics here are a little smaller than that of some classic compositions in literature. However, it is a good try to use Nd to form some novel perovskite solid solutions for capacity energy storage application.

In the present work, the (1-x)$Nd(Zn_{1/2}Ti_{1/2})O_3$–$xBaTiO_3$ ($0.0 \leq \times \leq 1.0$) composite ceramics were synthesized by a conventional solid-phase synthesis method. We studied the sintering behavior, microstructures, and the energy-storage properties of the $Nd(Zn_{1/2}Ti_{1/2})O_3$–$BaTiO_3$ ceramics.

## 2. Experimental

### 2.1. Preparation of the ceramics

The (1-x)$Nd(Zn_{1/2}Ti_{1/2})O_3$–$xBaTiO_3$ ($0.0 \leq \times \leq 1.0$) powders were synthesized by the conventional solid state reaction method. Proportionate amounts of reagent-grade starting materials of $BaCO_3$, ZnO (>99%, Sinopharm Chemical Reagen Co, Ltd, Shanghai, China), $Nd_2O_3$ (>99.99%, Sinopharm Chemical Reagen Co, Ltd, Shanghai, China) and $TiO_2$ (>99.95%, Yutong Chemical Reagents, Tianjin, China) were weighted according to the stoichiometric compositions of (1-x)$Nd(Zn_{1/2}Ti_{1/2})O_3$–$xBaTiO_3$ ($0.0 \leq \times \leq 1.0$). $Nd_2O_3$ powders were calcined at 1000 °C for 4 h before weighting. The mixed powders were milled in absolute ethyl alcohol solution with zirconia balls (2 mm in diameter) as milling media using polyethylene jars and planetary mill (QM-1F; Nanjing Machine Factory, Nanjing, China) for 4 h at a running speed of 150 rpm, then calcined in air at 1170 °C for 4 h. After being crushed and re-milled for 5 h at 200 rpm to increase reactivity and better homogeneity. Then the dried powders granulated with 5 wt% polyvinyl alcohol (PVA) were uniaxially pressed into cylinders (12 mm in diameter and 5 mm in height) in a steel die under pressure of 150 MPa. PVA was burnt out at 550 °C for 5 h (2 °C/min). Samples were sintered in the temperature ranges from 1300 °C to 1500 °C for 2 h (3 °C/min).

### 2.2. Characterization

Crystalline structures were investigated by using X-ray diffraction (XRD) with Cu Kα radiation (Rigaku D/MAX-2400 X-ray diffractometer, Tokyo, Japan). Microstructures were observed on fractured surfaces with scanning electron microscopy (SEM) (SEM; Quanta 250 F, FEI). Apparent densities were measured by Archimedes' method. To determine the dielectric properties, the sintered samples were polished and coated with silver on both surfaces. Temperature dependence of dielectric constant and loss was determined at frequencies between 100 Hz and 1 MHz by means of a LCR meter (HP 4980, Agilent, Palo Alto, CA) interfaced with a computer, where the specimens were heated at a rate of 2 °C/min from −100 °C to 350 °C. Polarization–electric field (P–E) hysteresis loops were measured at room temperature by a TF Analyzer 2000 (aix ACCT) ferroelectric test system. The electric field was applied from 1 to 140 kV/cm with a triangular wave form under 10 Hz during measurement.

## 3. Results and discussion

### 3.1. Structure of NZT–BT solid solutions

Fig. 1a and b shows the XRD patterns and lattice parameters of (1-x)$Nd(Zn_{1/2}Ti_{1/2})O_3$–$xBaTiO_3$ ($0.0 \leq \times \leq 1.0$) ceramics sintered at optimized sintering temperature, respectively. It is seen that all the samples crystallized into the polycrystalline perovskite structure and all the peaks are indexed based on the perovskite structure in Fig. 1a. As we can see from Fig. 1b, the lattice parameters and phase transition of (1-x)NZT-xBT ($0.0 \leq \times \leq 1.0$) ceramics are changed with x value increased. A complete perovskite solid solution is formed as x value increased from 0.0 to 0.3, a merging of characteristic reflection peaks, such as (011) and (101) peaks into a (110) peak is clearly observed. It can be seen that *a*, *b* and *c* decreases with x value increases. Since the ionic radii of $Ba^{2+}$ (1.61 Å) in 12

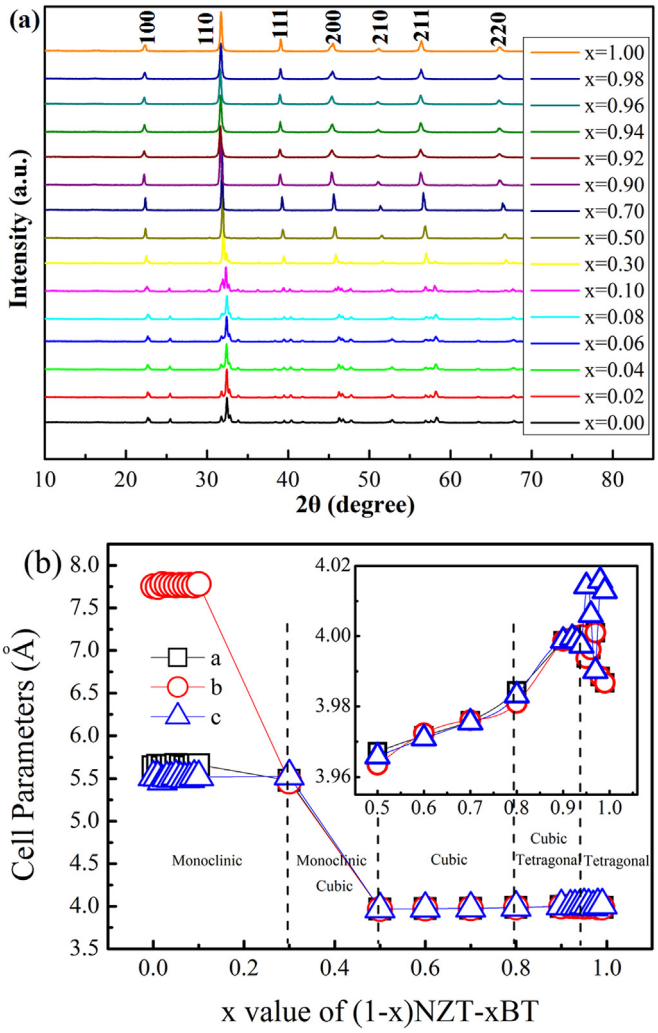


**Fig. 1.** XRD patterns (a) and lattice parameters (b) of the sintered (1-x)NZT–xBT ($0.0 \leq \times \leq 1.0$) ceramics.

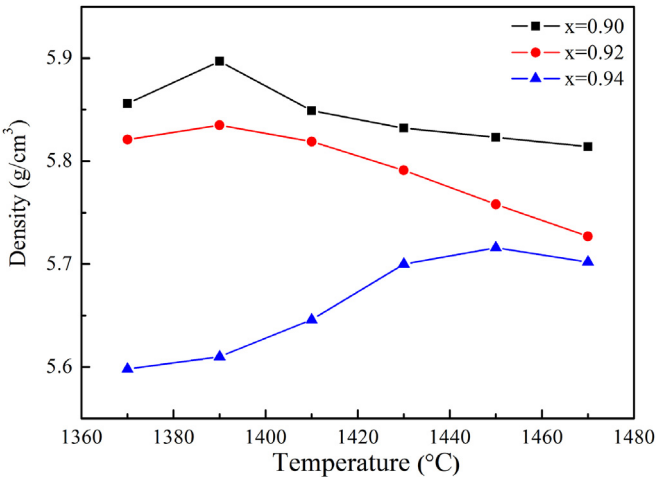


**Fig. 2.** The density of the (1-x)NZT-xBT ($0.90 \leq \times \leq 0.94$) ceramics as a function of sintering temperature for 2 h.

coordinate environment is a little larger than that of $Nd^{3+}$ (1.27 Å) and the (1-x)NZT-xBT ceramic with NZT phase (monoclinic structure). As seen from Fig. 1b, Crystal structures of the (1-x)NZT-xBT ceramics belong to cubic phase when $x \geq 0.5$, and it indicates that the phase transition from monoclinic to cubic structure with x value increased from 0.3 to 0.5. It can be seen that the ceramic possesses a single perovskite structure, and no appreciable secondary phase can be observed within $x \geq 0.6$, indicating that NZT can diffuse into the BT lattices to form a solid solution when $x \geq 0.6$. They become closer and closer and finally become equal to each other when $x = 0.6$ ($a = b = c = 3.9716(9)$ Å), which means that the crystal structure is changed from monoclinic to cubic phase. It indicates that a major phase of $BaTiO_3$ in (1-x)NZT-xBT ceramic when $x \geq 0.6$. As x value reaches 0.98, the crystal structure is changed from cubic to tetragonal phase with $a = 3.9867(0)$ Å, $b = 3.9867(0)$ Å, $c = 4.0128(3)$ Å.

### 3.2. Density measurements

Fig. 2 shows the relationships between sintering temperature and densities of the (1-x)$Nd(Zn_{1/2}Ti_{1/2})O_3$–x$BaTiO_3$ ($0.9 \leq \times \leq 0.94$) ceramics. As can be seen from Fig. 2, the bulk density of ceramics gradually increases and then decreases with increasing sintering temperature. Namely, it has a maximum value, which is called suitable sintering temperature (SST). It can be observed that the SST of NZT-BT ceramics decreases with increasing NZT content. The results indicate that NZT can lower the SST of $BaTiO_3$-based ceramics. Due to the density of pure NZT ceramic (6.89 g/cm$^3$) is higher than that of pure BT ceramics (6.01 g/cm$^3$), so the bulk density of NZN-BT is decreased with increasing BT content. From Fig. 2, the density of NZT-BT ceramics is about 5.6 g/cm$^3$ to 5.9 g/cm$^3$ at when $0.9 \leq \times \leq 0.94$.

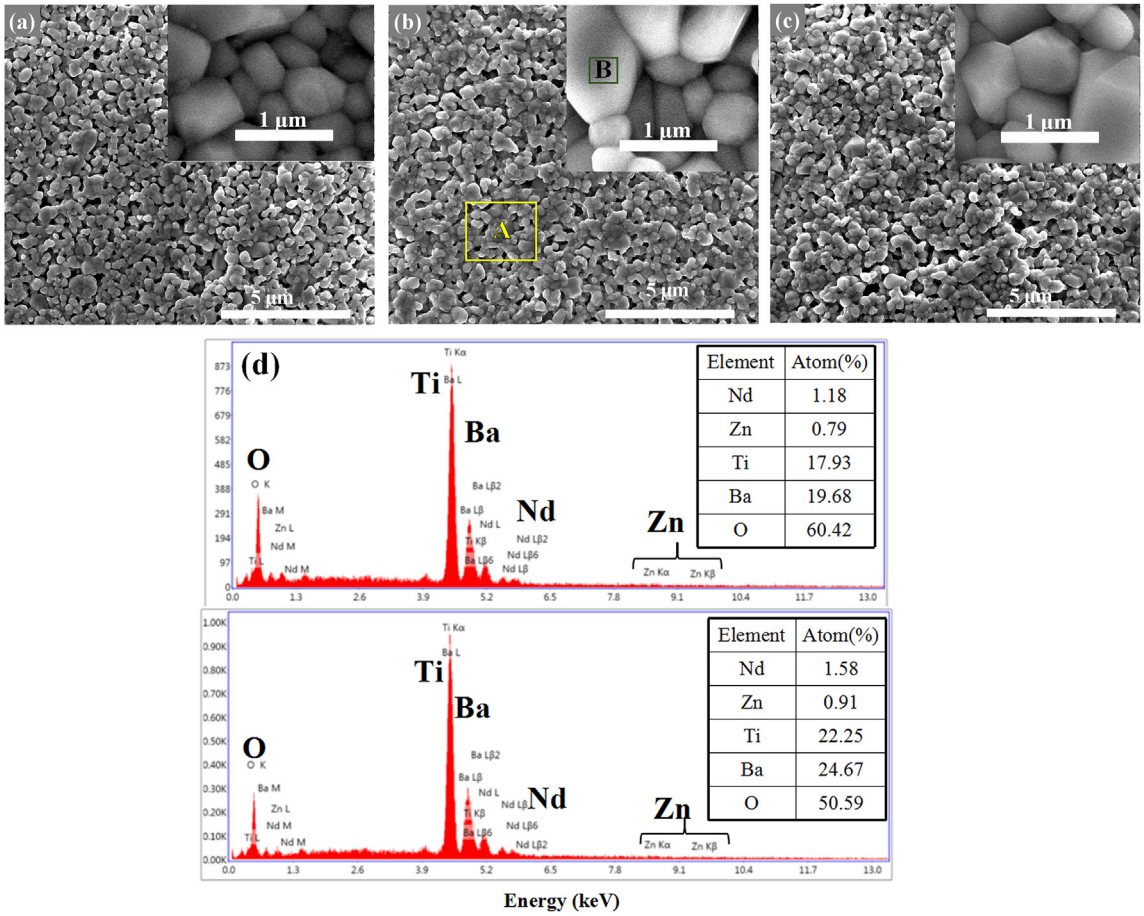


**Fig. 3.** SEM images and EDS analysis of the thermally etched surfaces of the (1-x)NZT-xBT ($0.90 \leq \times \leq 0.94$) ceramics sintered at: (a) x = 0.90; (b) x = 0.92; (c) x = 0.94; (d) EDS analysis of x = 0.92.

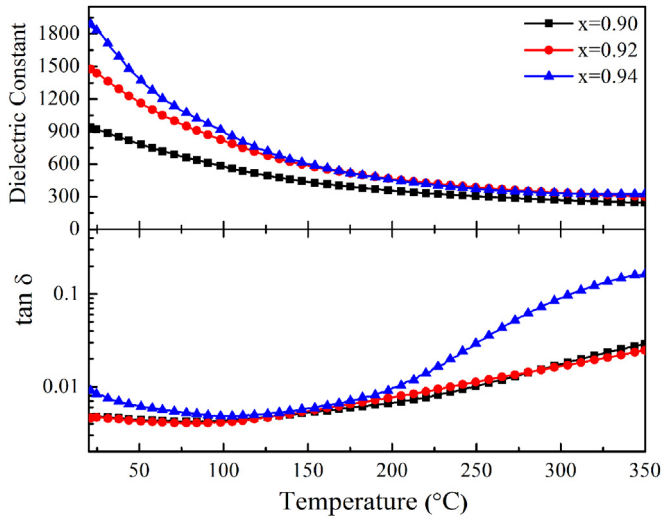


**Fig. 4.** Temperature dependence of dielectric constant and loss of the (1-x)NZT–xBT ($0.90 \leq \times \leq 0.94$) ceramics measured in the temperature range from 25 °C to 350 °C.

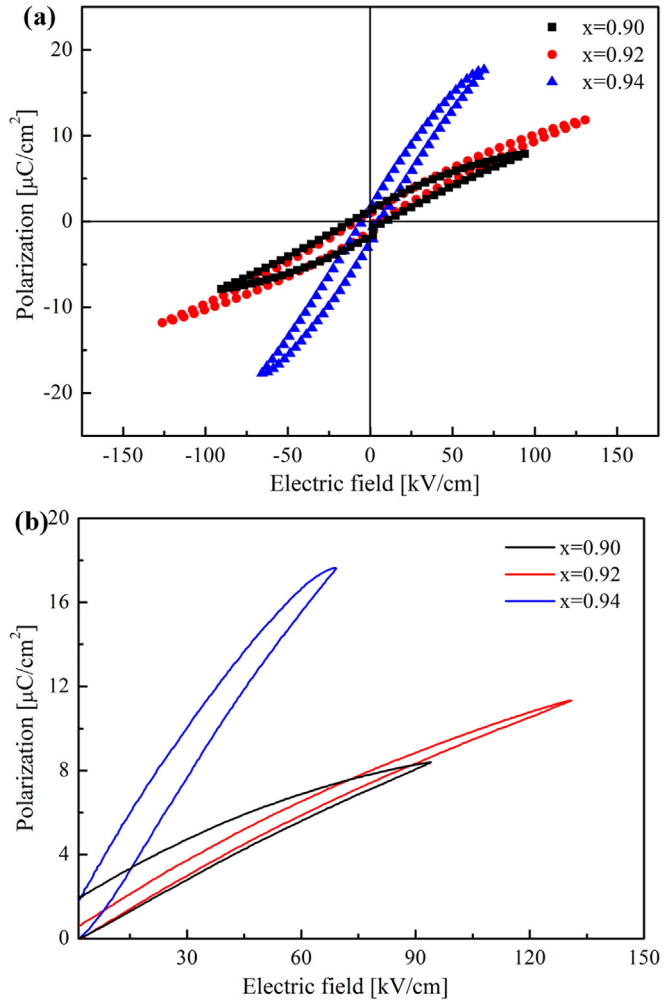


**Fig. 5.** The energy-storage properties of (1-x)NZT-xBT ceramics: (a) the bipolar P–E hysteresis loops at room temperatures, (b) the unipolar P–E hysteresis at room temperatures.

### 3.3. SEM results

Surface microstructure images and EDS analysis of the (1-x) $Nd(Zn_{1/2}Ti_{1/2})O_3$–$xBaTiO_3$ ($0.90 \leq \times \leq 0.94$) ceramics are shown in Fig. 3a–d. Evidently, with the content of BT increasing, grain sizes of samples does not change significantly. From Fig. 3a–c, the samples with different NZT concentration are densely sintered and grain sizes are homogeneous. Grain boundaries are clear, and no obvious visible pores can be found. The microstructure images correspond well with the densities analysis of samples. In order to confirm the chemical component content of these as-prepared ceramics, EDS analysis has been taken at some selected positions of the $0.08Nd(Zn_{1/2}Ti_{1/2})O_3$–$0.92BaTiO_3$ ceramic. Fig. 3d shows the composition analysis of a surface area (marked as A) and a single large grain (marked as B). It can be seen that the ratio of all elements in area of A and B are very close to the theoretical values of $0.08Nd(Zn_{1/2}Ti_{1/2})O_3$–$0.92BaTiO_3$, indicating that the chemical compositions are very average in the ceramics. The results of EDS analysis indicate that the NZT-BT solid solution was formed, which corresponds well with the XRD analysis above.

### 3.4. Dielectric properties

Fig. 4 shows temperature dependence of dielectric constant $\varepsilon_r$ and dielectric loss tanδ of the (1-x)$Nd(Zn_{1/2}Ti_{1/2})O_3$–$xBaTiO_3$ ($0.90 \leq \times \leq 0.94$) ceramics at 100 kHz. The curves show no evidence of dielectric peak from room temperature up to 350 °C. Dielectric constant of the samples decreased as temperature and show negative temperature coefficients of dielectric constant. Dielectric constant increases with increasing temperature and shows positive temperature coefficient of dielectric constant when the temperature reaches to 300 °C. To further understand the temperature dependence of dielectric constant $\varepsilon_r$ and dielectric loss tanδ of the (1-x)NZT–xBT ceramics, dielectric constant $\varepsilon_r$ and dielectric loss tanδ measured in the temperature range −100–150 °C are demonstrated in Fig. S1. As seen from Fig. S1, it can be seen that Curie temperature of (1-x)NZT-xBT ceramics increases from below −100 °C to 80 °C with increasing BT content. The dielectric constant and loss tangent of (1-x)NZT-xBT ceramics around the Curie temperatures are substantially reduced. Dielectric constant of the (1-x)NZT-xBT ceramics decreased with NZT content. It is attributed to the lower dielectric constant of NZT. Substitution of the $Ti^{4+}$ by $Zn^{2+}$ in the BT system resulted in weakening of bonding force between the B-site ion and oxygen ion of $ABO_3$ perovskite structure, leading to a reduced phase transition temperature ($T_C$), which is in consistence with earlier results that $T_C$ shifts to lower temperature with the substitution of the Ti-site by $Zn^{2+}$ in BT system [30].

### 3.5. Ferroelectric properties

Fig. 5 shows polarization–electric field (P–E) hysteresis loops of the (1-x)$Nd(Zn_{1/2}Ti_{1/2})O_3$–$xBaTiO_3$ ($0.90 \leq \times \leq 0.94$) ceramics were measured with 10 Hz unipolar triangle signal at room temperature. Energy storage behavior of the (1-x)NZT-xBT ceramics with different NZT content is calculated by P–E hysteresis loops. With increase of NZT content, P–E loop becomes flattened and slanted, indicating that the NZT addition weakens the ferroelectric properties of the ceramics remarkably. As NZT content increases further, the largest polarization decreases. The samples with higher NZT content exhibit linear P–E relationships. In general, the largest polarization of BT-based ceramics is increased effectively by addition of BT. Table 1 shows the maximum polarization ($P_{max}$), remnant polarization ($P_r$) of (1-x)$Nd(Zn_{1/2}Ti_{1/2})O_3$–$xBaTiO_3$ ceramics at room temperature. When x value increased from 0.9 to

**Table 1**
Maximum polarization ($P_{max}$), remnant polarization ($P_r$), dielectric breakdown field ($E_b$), discharge energy density, charge energy density and energy efficiency of (1-x)Nd($Zn_{1/2}Ti_{1/2}$)$O_3$–x$BaTiO_3$ ceramics at room temperature.

| x | Pmax (μC/cm$^2$) | Pr (μC/cm$^2$) | Eb (kV/cm) | Discharge energy density (J/cm$^3$) | Charge energy density (J/cm$^3$) | Energy efficiency (%) |
|---|---|---|---|---|---|---|
| 0.90 | 7.88 | 1.25 | 91 | 0.27 | 0.38 | 71.0 |
| 0.92 | 11.82 | 0.95 | 131 | 0.62 | 0.69 | 89.9 |
| 0.94 | 17.69 | 1.53 | 72 | 0.48 | 0.62 | 77.0 |

0.94, the largest polarization of the loop increased from 7.88 μC/cm$^2$ to 17.69 μC/cm$^2$. With the increase of BT content, ferroelectric properties of (1-x)NZT-xBT ceramic become stronger. Table 1 also shows the dielectric breakdown field ($E_b$), discharge energy density ($J_d$), charge energy density ($J_c$) and energy efficiency ($J_d/J_c$) of the NZT-BT ceramics. The charged energy density ($J_c$) of a dielectric material is equal to the integral of an area enclosed by charge curve and y-axis. The discharged energy density ($J_d$) is calculated by integrating the area enclosed by discharge curve and y-axis. The energy loss density is defined as the difference between charged and discharged energy densities, quantitatively equal to the inner space of P–E loop. Energy storage, energy loss and energy release of (1-x)NZT-xBT ceramics were calculated from the unipolar P–E hysteresis loops as described in Eq. (1). A maximum $J_c$ value of 0.62 J/cm$^3$ is achieved under 131 kV/cm at x = 0.92. The energy storage efficiency of the 0.08NZT-0.92BT ceramic was up to 90%.

## 4. Conclusion

In the present work, a series of (1-x)Nd($Zn_{1/2}Ti_{1/2}$)$O_3$–x$BaTiO_3$ ($0.0 \leq \times \leq 1.0$) ceramics were prepared by using conventional solid state reaction method. All the ceramic samples could be well densified at 1300 °C–1500 °C. XRD analysis indicated that a monoclinic solid solution region was formed in the range $0 < \times < 0.3$, a cubic perovskite solid solution was formed in the range $0.5 < \times < 0.9$, a tetragonal perovskite solid solution was formed in the range $0.94 < \times < 1$. The 0.08Nd($Zn_{1/2}Ti_{1/2}$)$O_3$–0.92$BaTiO_3$ ceramic sample was found to possess the largest energy density about 0.62 J/cm$^3$ with charging efficiency 90% at a breakdown field strength 131 kV/cm.

## Conflict of interest statement

The authors declare no competing financial interests.

## Acknowledgements

This work was supported by the Young Star Project of Science and Technology of Shaanxi Province (S2016YFXX0029), the Natural Science Foundation of Jiangsu Province (BK2014213), the Fundamental Research Funds for the Central University, the 111 Project of China (B14040), and the Department of Education of Guangdong Province of People's Republic of China (2014GKXM039). The SEM and EDS work was done at International Center for Dielectric Research (ICDR), Xi'an Jiaotong University, Xi'an, China and the authors thank Ms. Yan-Zhu Dai for her help in using SEM and EDS.

## Appendix A. Supplementary data

Supplementary data related to this article can be found at http://dx.doi.org/10.1016/j.jallcom.2016.05.311

## References

[1] G.R. Love, J. Am. Ceram. Soc. 73 (1990) 323–328.
[2] I. Burn, D.M. Smyth, J. Mater. Sci. 7 (1972) 339–343.
[3] J.J. Xu, Z.L. Wang, D. Xu, F.Z. Meng, X.B. Zhang, Energy Environ. Sci. 7 (2014) 2213–2219.
[4] Z.L. Wang, D. Xu, H.G. Wang, Z. Wu, X.B. Zhang, ACS Nano 3 (2013) 2422–2430.
[5] S. Kwon, W. Hackenberger, E. Alberta, E. Furman, M. Lanagan, IEEE Electr. Insul. Mag. 27 (2011) 43–55.
[6] X.L. Huang, D. Xu, S. Yuan, D.L. Ma, S. Wang, H.Y. Zheng, X.B. Zhang, Adv. Mater. 26 (2014) 7264–7270.
[7] S. Yuan, X.L. Huang, D.L. Ma, H.G. Wang, F.Z. Meng, X.B. Zhang, Adv. Mater. 26 (2014) 2273–2279.
[8] J. Kuwata, K. Uchino, S. Nomura, Ferroelectrics 22 (1979) 863–867.
[9] J. Wang, K. Li, H.X. Zhong, D. Xu, Z.L. Wang, Z. Jiang, Z.J. Wu, X.B. Zhang, Angew. Chem. Int. Ed. 54 (2015) 10530–10534.
[10] K. Yao, S. Chen, M. Rahimabady, M.S. Mirshekarloo, S. Yu, F.E.H. Tay, T. Sritharan, L. Lu, IEEE Trans. Ultrason. Ferroelectr. Freq. Control 58 (2011) 1968–1974.
[11] S.M. Xiu, S. Xiao, W.Q. Zhang, S.X. Xue, B. Shen, J.W. Zhai, J. Alloys Compd. 670 (2016) 217–221.
[12] X.L. Huang, R.Z. Wang, D. Xu, Z.L. Wang, H.G. Wang, J.J. Xu, Z. Wu, Q.C. Liu, Y. Zhang, X.B. Zhang, Adv. Funct. Mater. 23 (2013) 4345–4353.
[13] B.Y. Wang, L.H. Luo, X.J. Jiang, W.P. Li, H.B. Chen, J. Alloys Compd. 585 (2014) 14–18.
[14] B.B. Liu, X.H. Wang, Q.C. Zhao, L.T. Li, J. Am. Ceram. Soc. 98 (2015) 2641–2646. JACC.
[15] S. Yuan, Y.B. Liu, D. Xu, D.L. Ma, S. Wang, X.H. Yang, Z.Y. Cao, X.B. Zhang, Adv. Sci. 2 (2015) 1400018.
[16] R. Dittmer, W. Jo, D. Damjanovic, J. Rödel, J. Appl. Phys. 109 (2011) 034107.
[17] X.R. Cheng, M.R. Shen, Solid State Commun. 141 (2007) 587–590.
[18] Y.Y. Zhao, J.W. Xu, L. Yang, C.R. Zhou, X.P. Lu, C.L. Yuan, Q.N. Li, G.H. Chen, H. Wang, J. Alloys Compd. 666 (2016) 209–216.
[19] X.Y. Wei, H.X. Yan, T. Wang, Q.Y. Hu, G. Viola, S. Grasso, Q.H. Jiang, L. Jin, Z. Xu, M.J. Reece, J. Appl. Phys. 113 (2013) 024103.
[20] D. Zhan, Q. Xu, D.P. Huang, H.X. Liu, W. Chen, F. Zhang, J. Alloys Compd. 682 (2016) 594–600.
[21] C.C. Huang, D.P. Cann, J. Appl. Phys. 104 (2008) 024117.
[22] R.A. Malik, A. Hussain, A. Maqbool, A. Zaman, T.K. Song, W.J. Kim, M.H. Kim, J. Alloys Compd. 682 (2016) 302–310.
[23] J.B. Zhao, H.L. Du, S.B. Qu, J.F. Wang, H.M. Zhang, Y.M. Yang, Z. Xu, J. Alloys Compd. 509 (2011) 3537–3540.
[24] T. Wang, X.Y. Wei, Q.Y. Hu, L. Ji, Z. Xu, Y.J. Feng, Mater. Sci. Eng. B 178 (2013) 1081–1086.
[25] G.C. Liu, H.Q. Fan, G.Z. Dong, J. Shi, Q. Chang, J. Alloys Compd. 655 (2016) 632–638.
[26] X.C. Wang, J. Shen, T.Q. Yang, Y. Dong, Y.Z. Liu, J. Alloys Compd. 655 (2016) 309–313.
[27] Q. Li, J. Wang, Y. Ma, L.T. Ma, G.Z. Dong, H.Q. Fan, J. Alloys Compd. 663 (2016) 701–707.
[28] H. Ogihara, C.A. Randall, S. Trolier-Mckinstry, J. Am. Ceram. Soc. 92 (2009) 1719–1724.
[29] G.Z. Zhang, D.Y. Zhu, X.S. Zhang, L. Zhang, J.Q. Yi, B. Xie, Y.K. Zeng, Q. Li, Q. Wang, S.L. Jiang, J. Am. Ceram. Soc. 98 (2015) 1175–1181.
[30] C.M. Wu, W.J. Chen, Y. Zheng, D.C. Ma, B. Wang, J.Y. Liu, C.H. Woo, Sci. Rep. 4 (2014) 3946.
[31] P. Zheng, J.L. Zhang, Y.Q. Tan, C.L. Wang, Acta Mater. 60 (2012) 5022–5030.
[32] C.F. Tseng, C.L. Huang, W.R. Yang, J. Am. Ceram. Soc. 89 (2006) 1465–1470.